CHEMISTRY OF MATERIALS
Cite This: Chem. Mater. 2018, 30, 8359−8367
Article
pubs.acs.org/cm

Facile Exchange of Tightly Bonded L-Type Oleylamine and Diphenylphosphine Ligands on Copper Indium Diselenide Nanocrystals Mediated by Molecular Iodine

Daniel W. Houck and Brian A. Korgel*

McKetta Department of Chemical Engineering and Texas Materials Institute, The University of Texas at Austin, Austin, Texas 78712, United States

Supporting Information

ABSTRACT: Copper indium diselenide ($CuInSe_2$) nanocrystals are a prototypical I−III−VI semiconductor quantum dot material, typically synthesized in oleylamine (OLAm) as a solvent and capping ligand, often with the addition of diphenylphosphine (DPP) to improve the reaction yield. Using ^1H nuclear magnetic resonance spectroscopy, we study the association of OLAm and DPP on $CuInSe_2$ nanocrystals and find that they both behave as tightly bonded L-type ligands. There is no observable desorption of OLAm or DPP when a toluene-d_8 dispersion is heated to 100 °C, and no ligand exchange occurs when the nanocrystals are exposed to other L-type species like trioctylphosphine (TOP) or octadecanethiol (ODT), which can bind as either X-type or L-type. Molecular iodine (I_2), however, is found to readily displace both OLAm and DPP from the nanocrystal surface and facilitate efficient and complete ligand exchange with either TOP or ODT and appears to behave as a Lewis acid Z-type ligand. We also find that the X-type ligand, stearic acid, does not bond to the $CuInSe_2$ nanocrystals under any circumstances.

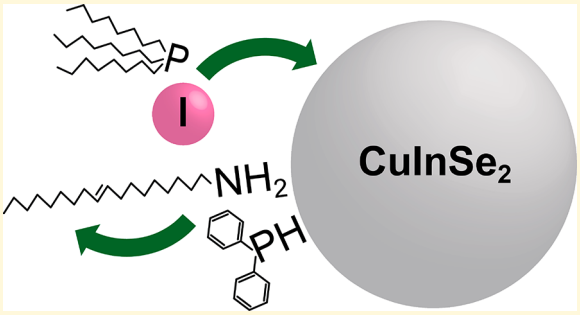

INTRODUCTION

Nanocrystals made of I−III−VI semiconductors, such as $CuInSe_2$, have been of significant interest in the past decade.[1−18] Ligand-capped $CuInSe_2$ nanocrystals can be synthesized as efficient light emitters[19,20] or formulated into inks for fabrication of the light-absorbing layer in photovoltaic devices (PVs).[21−23] Understanding the physical and chemical relationships between nanocrystals and their organic ligand shell underlies the development of electronic and optoelectronic devices based on these materials.[24] The organic ligands provide colloidal stability, which has enabled the fabrication of PVs on unique substrates like paper[25] and grooves in plastic[26] that cannot withstand high-temperature processing; however, the performance of PVs made with $CuInSe_2$ nanocrystals without high-temperature selenization has been limited by poor charge transport because of the organic ligands in the film.[21,27,28] In the case of PbS nanocrystals, high-performance PVs have been made by modifying the capping ligand layer using various ligand exchange processes with thiols, ammonium salts, and halides.[29−33] In one case, addition of I_2 to PbS nanocrystals helped to improve PV device performance.[34] Ligands have been exchanged on $CuInSe_2$ nanocrystals for improved electrical conductivity and photoconductivity in deposited layers, but ligand exchange has not resulted in significant improvements in PV performance.[26,27,35,36] One problem is that ligand bonding on $CuInSe_2$ nanocrystals has not been studied to any significant extent.

For a wide variety of nanocrystals, including CdSe,[37−41] PbSe,[42] metal oxides,[43,44] $CsPbBr_3$,[45] CuS,[46] and $CuInS_2$,[47] ligand bonding has been effectively described by covalent bond classification (CBC), thus providing fundamental insight into how ligand exchange proceeds on these nanocrystals.[48,49] Ligands are designated as X-type, L-type, or Z-type, depending on how many electrons are donated to the nanocrystal−ligand bond, and ligands can be exchanged only when charge neutrality is maintained.[37,48] Amines and phosphines are L-type, acting as Lewis bases that bond to Lewis acid sites by a dative bond that donates two electrons to the nanocrystal surface. Carboxylates are X-type ligands that donate one electron to the nanocrystal surface to form a covalent bond. Z-Type ligands act as Lewis acids and coordinate with the nanocrystal surface by accepting two electrons to form a dative bond, as in the case of $Cd(oleate)_2$.[49] Typically, ligands must be of the same type to readily exchange;[50] however, charge neutral L-type and Z-type ligands have also been found to readily exchange in some cases.[51,52]

Here, we show using ^1H nuclear magnetic resonance (NMR) spectroscopy that the native L-type ligands on $CuInSe_2$ nanocrystals, oleylamine (OLAm) and diphenylphosphine (DPP), do not readily exchange with other L-type ligands, such as trioctylphosphine (TOP), as might be

Received: September 21, 2018
Revised: November 5, 2018
Published: November 6, 2018

DOI: 10.1021/acs.chemmater.8b04016
Chem. Mater. 2018, 30, 8359−8367

expected on the basis of the CBC and the law of mass action.[50,53−56] Similar tight ligand binding has been observed for amines and thiols on $CuInS_2$ nanocrystals.[46,47,57] NMR spectroscopy has been used widely to examine ligand binding to nanocrystals in a variety of systems.[47,56,58,59] We also show that the addition of I_2 to the $CuInSe_2$ nanocrystal dispersion facilitates desorption of OLAm and DPP and enables facile ligand exchange with TOP. We propose that I_2 acts as a Z-type ligand in which the I adatom forms a dative bond with the nanocrystal surface. This mechanism is consistent with reports indicating that Z-type and L-type ligands can participate in facile ligand exchange[51,52] and the observed binding of I_2 to $CuInSe_2$ surfaces.[60] These results support the findings that L-type and Z-type ligands can participate in facile exchange and indicate that Z-type ligands can even induce exchange between two L-type ligands.

EXPERIMENTAL SECTION

Materials. Copper(I) chloride (CuCl, 99.99%), elemental selenium powder (Se, 99.99%), anhydrous toluene (99.8%), oleylamine (OLA, ≥98%), diphenylphosphine (DPP, 98%), octadacanethiol (ODT, 98%), stearic acid (StAc 98.5%), and iodine (I_2 ≥ 99.8%) were obtained from Sigma-Aldrich. Copper, indium, and selenium standard solutions for inductively coupled plasma-atomic emission spectroscopy (ICP-AES) with concentrations of 1 mg/mL and 70% wt nitric acid were obtained from Sigma-Aldrich. Indium chloride ($InCl_3$, 99.99%) was obtained from Strem Chemical. Toluene, ethanol, and deuterated chloroform (chloroform-*d*) with 0.05% (v/v) tetramethylsilane (TMS) were obtained from Fisher Scientific. OLAm was degassed before use by maintaining vacuum under 200 mTorr for 4 h at 110 °C and stored in a nitrogen-filled glovebox. All other chemicals were used as received.

$CuInSe_2$ Nanocrystal Synthesis. $CuInSe_2$ nanocrystals were synthesized using a variation of a previously published method.[61] In a nitrogen-filled glovebox, 5 mmol (0.49 g) of CuCl, 5 mmol (1.11 g) of $InCl_3$, and 50 mL of OLAm were loaded into a three-neck flask. Selenium (10 mmol, 0.79 g) was dissolved in 10 mL of diphenylphosphine (DPP). The OLAm-containing flask was transferred to a Schlenk line and heated to 110 °C for 30 min in vacuum (200 mTorr) to dissolve the metal salts. The flask was then placed under a nitrogen atmosphere, and the temperature was increased to 240 °C over 10 min. The DPP/Se solution was injected into the flask during the temperature ramp at 180 °C. The reaction mixture was held at 240 °C for 1 h and then allowed to cool to room temperature by removing the heating mantel. $CuInSe_2$ nanocrystals were isolated from the reaction mixture by precipitation with 20 mL of ethanol followed by centrifugation (2600 rcf for 10 min). The supernatant was discarded, and the black precipitate was redispersed in 10 mL of toluene. The nanocrystals were precipitated again with 5 mL of ethanol followed by centrifugation (2600 rcf for 10 min). The supernatant was discarded, and the nanocrystals were dispersed in toluene and centrifuged again (2600 rcf for 10 min) to remove poorly capped particles. The nanocrystal product was dried by rotary evaporation, transferred into a nitrogen-filled glovebox, and dispersed in anhydrous toluene to ensure that the nanocrystals were not oxidized prior to the ligand exchange experiments. This reaction yielded 1.4 g of dispersible nanocrystal product.

Ligand Exchange. All ligand exchange experiments were performed in a nitrogen-filled glovebox. A stock solution with 100 mg/mL $CuInSe_2$ nanocrystals dispersed in toluene was prepared for all ligand exchanges. This corresponds to a nanocrystal concentration of 5×10^{-5} M and a bound ligand (OLAm) concentration of ∼40 mM. A stock solution of 60 mg/mL (0.24 M) I_2 in toluene was also prepared. Ligand exchanges were then performed by combining 1.5 mL of the $CuInSe_2$ nanocrystal dispersion with 2 mL of additional free ligand species and the desired amount of I_2 solution and toluene. The final exchange solutions included 150 mg of $CuInSe_2$, 2.5 mL of toluene, 2 mL of free ligand, and various amounts of I_2. After the ligand exchange, 5 mL of ethanol was added to the solution to aggregate the nanocrystals and quench the exchange. The nanocrystals were isolated by centrifugation, and the clear supernatant was discarded. The nanocrystals were redispersed in 1 mL of toluene and precipitated again by adding 0.5 mL of ethanol and centrifuging. The supernatant was discarded, and the purified, ligand-treated, nanocrystals were dispersed in 1 mL of toluene and centrifuged to remove any poorly capped particles. In a typical ligand exchange with 0.5 mL of the I_2 solution (30 mg or 0.12 mmol of I_2), nearly complete ligand exchange occurred with a product yield of 55 wt % for the nanocrystals retaining their colloidal stability. This corresponds to approximately four iodine atoms per bound OLAm molecule.[62]

Analysis. ^{1}H NMR spectra were measured for nanocrystals dispersed in deuterated chloroform (chloroform-*d*) at a concentration of 50 mg/mL in a 5 mm NMR tube. ^{1}H NMR spectra were recorded using an Agilent MR 400 spectrometer operating at 400 MHz (9.4 T), using a 90° pulse width, a 2 s relaxation delay, and 128 scans. Data were processed using MestReNova software for background correction and alignment of the residual solvent peak. With *in situ* heating, ^{1}H NMR spectra were collected with nanocrystals dispersed in deuterated toluene (toluene-d_8) using 64 scans at each temperature. For the ^{1}H NMR *in situ* heating experiments, spectra were acquired as the temperature was increased in 20 °C increments to 100 °C, and then a final measurement was taken after the dispersion had been cooled back to 25 °C. When I_2 solutions were added to NMR samples, a 60 mg/mL (0.24 M) solution of I_2 in chloroform-*d* was prepared and 0.083 mL of this I_2 solution (5 mg or 0.02 mmol of I_2) was added to 1.0 mL of a 50 mg/mL nanocrystal solution in chloroform-*d*.

X-ray diffraction (XRD) data were collected with a Rigaku R-Axis Spider diffractometer operated at 40 kV and 40 mA using an image-plate detector with Cu Kα (λ = 1.54 Å) radiation. Dried nanocrystal powder was suspended in a 0.5 mm nylon loop. The samples were scanned for 10 min while rotating at 2°/s. The two-dimensional powder diffraction patterns were converted to the reported one-dimensional XRD patterns with the Rigaku 2DP powder processing program.

Transmission electron microscopy (TEM) images were digitally acquired using an FEI Tecnai transmission electron microscope at an 80 kV accelerating voltage. Nanocrystals were prepared for TEM imaging by drop casting. Nanocrystals were dispersed at a concentration of 0.125 mg/mL in toluene and evaporated onto a carbon-coated mesh nickel TEM grid.

X-ray photoelectron spectroscopy (XPS) was performed with a Kratos XPS instrument using a high-intensity monochromatic Al Kα X-ray source and a 180° hemispherical electron energy analyzer. The collected spectra were processed with CasaXPS software. Sample charging was corrected by shifting the C 1s peaks to a value expected of hydrocarbons at 284.8 eV. For quantification, baseline subtraction of the spectra was performed using a Shirley background, and the peaks were integrated.[63−65] Each peak area was divided by the corresponding relative sensitivity factor (RSF) in the Kratos library and then normalized to yield the surface sensitive sample composition estimate. Nanocrystals were prepared for XPS by spin coating toluene (50 mg/mL) dispersions onto a conductive boron-doped silicon wafer (ρ = 0−10 Ω cm). The samples were loaded onto the sample holder with conductive copper tape and grounded with conductive carbon tape to prevent charging.

The elemental composition of the nanocrystals was determined using ICP-AES on a Varian 710 ICP-AES instrument. Samples were prepared by dissolving ∼5 mg of $CuInSe_2$ nanocrystals in 1 mL of 70% (v/v) nitric acid followed by dilution with doubly distilled deionized water. Three replicates of the measurements were taken, and the Cu 213.598, In 230.606, and Se 196.026 emission lines were used because they had the lowest deviation between replicates. The reported error is the standard deviation of the replicates.

DOI: 10.1021/acs.chemmater.8b04016
Chem. Mater. 2018, 30, 8359−8367

RESULTS AND DISCUSSION

$CuInSe_2$ nanocrystals with diameters of 8−14 nm were prepared by heating diphenylphosphine selenide (DPP-Se) with CuCl and $InCl_3$ in OLAm. In this reaction scheme, OLAm serves as the primary source of ligands, while DPP serves as a catalyst for nanocrystal synthesis that significantly improves the yield of the reaction.[61] Measurement of the elemental composition by ICP-AES showed that the nanocrystals are copper poor (0.8:1.06:2 Cu:In:Se) yet charge neutral within ICP error with the chalcopyrite crystal structure. Figure 1 shows ^{1}H NMR spectra of purified nanocrystals in

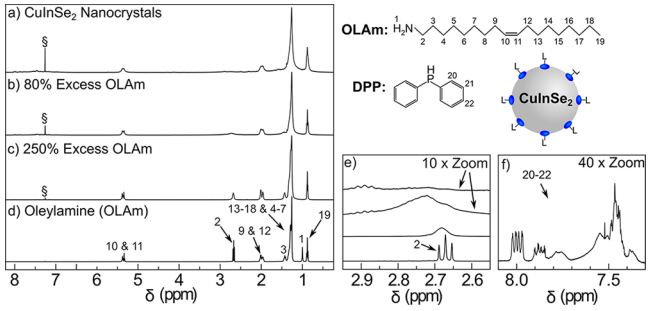

Figure 1. ^{1}H NMR spectra of (a) purified $CuInSe_2$ nanocrystals capped with OLAm, (b) $CuInSe_2$ nanocrystals with 80% excess OLAm (0.01 mL of OLAm added per 100 mg of $CuInSe_2$), (c) $CuInSe_2$ nanocrystals with 250% excess OLAm (0.03 mL of OLAm added per 100 mg of $CuInSe_2$), and (d) pure OLAm in chloroform-*d*. (e) Region of panels a−d corresponding to the protons closest to the nanocrystal's surface (peak 2), with the top two curves magnified (10×) for the sake of clarity. (f) Magnification of the spectra in panel a corresponding to the aromatic hydrogens of DPP δ 7.5−8.0 ppm. The "% excess OLAm" is determined by measuring the amount of OLAm in the dispersion from the relative NMR signal intensities of the vinylic hydrogen of OLAm at δ 5.36 ppm and the TMS standard peak at δ 0 ppm.

chloroform-*d*. The spectra have broadened methyl δ 0.88 ppm and methylene δ 1.25 ppm resonances characteristic of OLAm bound to the $CuInSe_2$ nanocrystal surface. Peak broadening in ^{1}H NMR spectra of capping ligands results from the restricted motion of the molecules, especially those embedded deeper within the capping ligand layer near the nanocrystal surface.[66−68] Resonances corresponding to the vinylic hydrogens of OLAm δ 5.36 ppm and the hydrogens neighboring the double bond δ 2.00 ppm are also observed. Additional sharp resonances at δ 1.00 ppm, δ 2.67 ppm, and δ 1.43 ppm corresponding to hydrogens associated with the amine group, α-hydrogens, and β-hydrogens, respectively, which are distinctly observed in solutions of free OLAm are not present in the spectra. These resonances have the most restricted molecular motion and therefore are not observed in the spectra of the purified nanocrystals because of their significant peak broadening,[69] further indicating that all of the OLAm in the nanocrystal dispersion is bonded to $CuInSe_2$ nanocrystals (see the Supporting Information for ^{1}H NMR spectra of all ligand species in this study). As shown in Figure 1, the peaks related to OLAm in the ^{1}H NMR spectra sharpen and become more intense when OLAm is added to the nanocrystal dispersion. The ^{1}H NMR spectra in Figure 1 also indicate that DPP is incorporated into the capping ligand layer. Although the signal is weaker than the OLAm resonances, broadened resonances corresponding to the aromatic hydrogens of DPP δ 7.5−8.0 ppm are visible (Figure 1f).

Using an approach similar to that of Hens and co-workers,[47] we examined the ligand dissociation kinetics of OLAm and DPP on $CuInSe_2$ nanocrystals by heating a dispersion of nanocrystals in toluene-d_8 *in situ* and monitoring the ^{1}H NMR spectra for peak sharpening as evidence of desorption. Toluene-d_8 was used as the solvent for these experiments because it provides a wider temperature window than chloroform-*d* does because of its higher boiling point. Figure 2 shows the ^{1}H NMR spectra of a $CuInSe_2$ nanocrystal

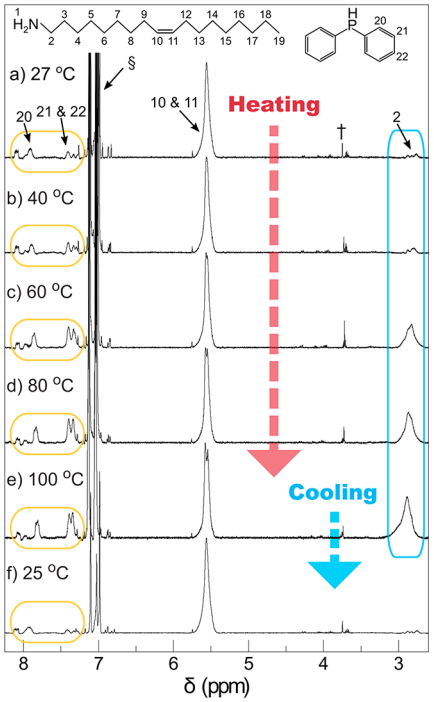

Figure 2. *In situ* ^{1}H NMR spectra of $CuInSe_2$ nanocrystals heated in toluene-d_8 at (a) 27, (b) 40, (c) 60, (d) 80, and (e) 100 °C. (f) Spectra of the dispersion after it had been cooled back to room temperature. § indicates the solvent (toluene-d_8) signal, and † denotes an impurity peak consistent with trace amounts of 2-propanol. The complete NMR spectra are provided in Figure S2.

dispersion heated to 100 °C and then cooled back to room temperature. As the temperature increases, all of the peaks narrow from the increased levels of molecular motion of the ligands. This sharpening is most apparent for the peaks corresponding to protons near the nanocrystal surface for which the restricted molecular motion is most extreme. After the sample had been cooled back to room temperature, the ^{1}H NMR spectra were identical to the spectra before heating. These data indicate that the ligands do not desorb at elevated temperatures in the time frame of the measurement and that the ligands are strongly bonded. Another confirmation that the ligands remain bound to the nanocrystals at elevated temperatures was the lack of any observed precipitation.

An exchange of OLAm and DPP ligands was attempted with 150 mg of nanocrystals dispersed in 1.5 mL of toluene with the addition of 2 mL (4.5 mmol) of TOP. This corresponds to a nanocrystal concentration of 1.4×10^{-5} M and a bound ligand concentration of ~15 mM. These ligand exchange conditions correspond to an extreme excess of TOP, with roughly 100 times more free TOP than nanocrystal-bound native OLAm

DOI: 10.1021/acs.chemmater.8b04016
Chem. Mater. 2018, 30, 8359−8367

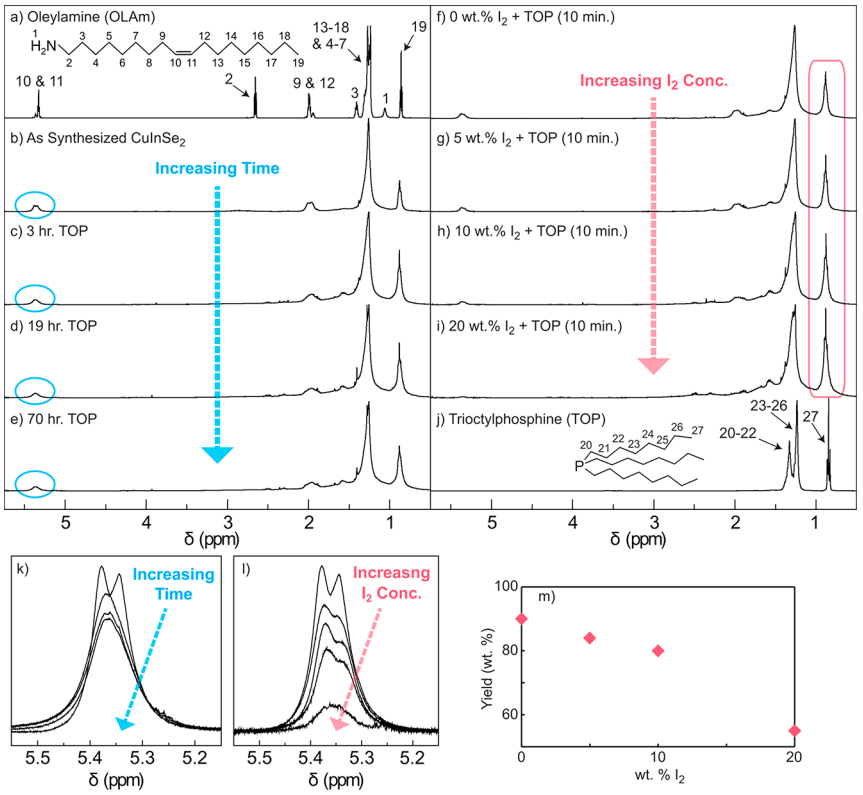

Figure 3. ^{1}H NMR spectra of $CuInSe_2$ nanocrystals dispersed in chloroform-*d* after various ligand exchange procedures and subsequent purification. (a) Pure OLAm for reference. (b) Purified $CuInSe_2$ nanocrystal dispersion prior to exposure to any exchange solution. (c–e) Purified $CuInSe_2$ nanocrystal dispersions after exposure to excess TOP for 3, 19, and 70 h, respectively. (f–i) Purified $CuInSe_2$ nanocrystals after a 10 min exposure to excess TOP and 0, 5, 10, and 20 wt % I_2, respectively. (k) Regions corresponding to the OLAm double bond in panels b–e overlaid, indicating no OLAm removal with increased TOP exposure time. (l) Regions corresponding to the OLAm double bond in panels b and f–i overlaid, indicating that the OLAm is removed during exchanges performed in the presence of I_2. (m) Percent yield by mass of dispersible product plotted against the amount of I_2 added to the 3 h ligand exchange solution.

and DPP. After exposure to TOP for 3, 19, and 70 h at room temperature, the nanocrystals were purified with two isolative precipitation steps and redispersed in chloroform-*d* to obtain ^{1}H NMR spectra. Panels a–e of Figure 3 show the ^{1}H NMR spectra. The peaks corresponding to hydrogens located near the double bond in OLAm at δ 2.0 and 5.35 ppm are still clearly observed with intensities relative to the methyl and methylene signals that remain relatively unchanged and independent of exchange time, indicating that OLAm desorption, and the associated TOP adsorption, has not occurred to any significant extent. Similarly, a test of ligand exchange using octadecanethiol (ODT) resulted in no observable change in the ^{1}H NMR spectra of the nanocrystals, as shown in panels a and b of Figure 4.

A similar difficulty in achieving complete ligand exchange has been observed in $CuInS_2$ nanocrystals, where native OLAm ligands are only partially exchanged with thiols.[47] X-Type oleic acid ligands bound to CdSe nanocrystals also exhibit tight binding behavior and will not spontaneously desorb when exposed to an excess of phosphonic acid.[38] Exchange between X-type oleic acid and L-type tri-*n*-butylphosphine can, however, be facilitated on CdSe nanocrystals when mediated by chlorotrimethylsilane.[39]

In the process of attempting a variety of ligand exchanges, we found that molecular iodine (I_2) induces rapid desorption of OLAm and DPP capping ligands from $CuInSe_2$ nanocrystals. Figure 5 shows ^{1}H NMR spectra of $CuInSe_2$ nanocrystals exposed to I_2. Shortly after (<1 h) the addition of I_2 to a

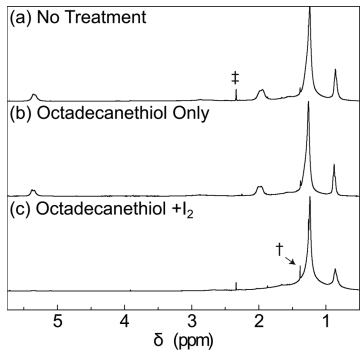

Figure 4. ^{1}H NMR spectra of as-synthesized $CuInSe_2$ nanocrystals (a) as synthesized, (b) after a 70 h exposure to ODT at room temperature without I_2, and (c) after exposure to ODT at room temperature in the presence of 20% wt I_2 for 10 min. The disappearance of the peaks corresponding to the OLAm double bond at δ 5.36 and 2.00 ppm corresponding the vinylic hydrogens and hydrogens neighboring the double bond indicates that OLAm is replaced with ODT on the nanocrystal surface. † and ‡ denote impurity peaks consistent with trace amounts of acetone and water, respectively.

dispersion of $CuInSe_2$ nanocrystals, the ^{1}H NMR spectra exhibit sharp peaks at δ 7.5–8.0 ppm corresponding to the hydrogens associated with the phenyl groups in DPP and δ 2.85–2.95 ppm corresponding to the hydrogens neighboring the amine group of OLAm, indicating that a significant amount of capping ligands has desorbed from the nanocrystal surface.

DOI: 10.1021/acs.chemmater.8b04016
Chem. Mater. 2018, 30, 8359–8367

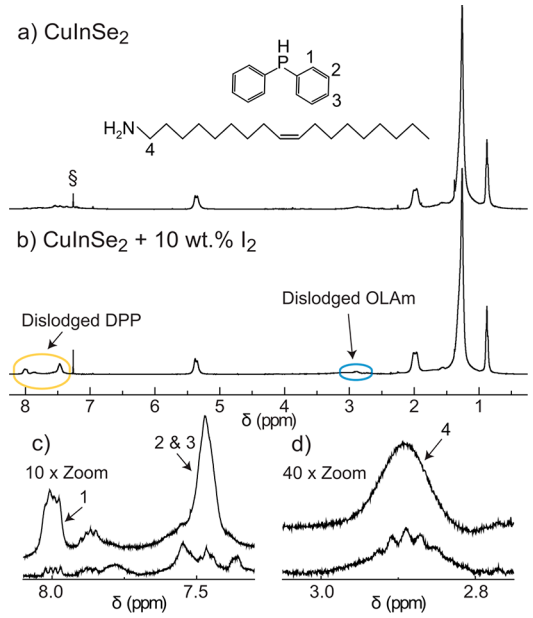

Figure 5. ^{1}H NMR spectra of $CuInSe_2$ nanocrystals dispersed in chloroform-*d* after exposure to I_2 indicating the desorption of OLAm and DPP ligands. (a) Purified $CuInSe_2$ nanocrystal dispersion. (b) $CuInSe_2$ nanocrystal dispersion after the addition of 10% wt I_2. (c) Regions of panels a (bottom) and b (top) corresponding to the aromatic protons in DPP magnified 10 times. (d) Regions of panels a (bottom) and b (top) corresponding to the protons closest to the NH_2 group in OLAm magnified 40 times. § indicates the solvent signal (chloroform-*d*).

Consequently, we tried to exchange the OLAm and DPP capping ligands with TOP and ODT using I_2 to enhance the process. Nanocrystals were dispersed in the presence of TOP and I_2, or ODT and I_2, for 10 min and then recovered, purified, and dispersed in chloroform-*d* to obtain the ^{1}H NMR spectra shown in Figures 3 and 4. Panels f–i of Figure 3 show the ^{1}H NMR spectra of solutions of nanocrystals dispersed in excess TOP when exposed to various concentrations of I_2. Higher concentrations of I_2 led to more complete exchange of OLAm with TOP, indicated by the disappearance of the resonances characteristic of OLAm near the double bond at δ 5.4 and 2.0 ppm. The exchange with TOP is further indicated by the increased relative intensity of the methyl-related resonance at δ 0.88 ppm, consistent with the greater number of methyl groups per molecule of TOP than of OLAm. Increasing the I_2 concentration too much led to a decrease in the amount of the dispersible nanocrystal product, as shown in Figure 3m. In the extreme case, 1:1 addition by weight of I_2 to $CuInSe_2$ nanocrystals led to the complete degradation of the nanocrystals to a red solid composed of $CuISe_3$, as shown in the Supporting Information. Fourier-transform infrared spectroscopy (FTIR) was also used on the $CuInSe_2$ samples exchanged with I_2 and TOP to confirm that complete ligand exchange had occurred. The NH_2 bend at 1600 cm^{-1} has disappeared from the FTIR spectra (see Figure S4), confirming that the amines have been removed from the nanocrystal surface. A similar exchange procedure was successfully used to exchange OLAm with ODT, indicated by the ^{1}H NMR spectra in Figure 4. The resonances characteristic of OLAm near the double bond at δ 5.4 and 2.0 ppm are no longer present in the spectra, indicating that the addition of I_2 led to the complete ligand exchange of OLAm for ODT.

As shown in Figure 6, TEM and XRD of the ligand-exchanged nanocrystals also show they retain their crystal

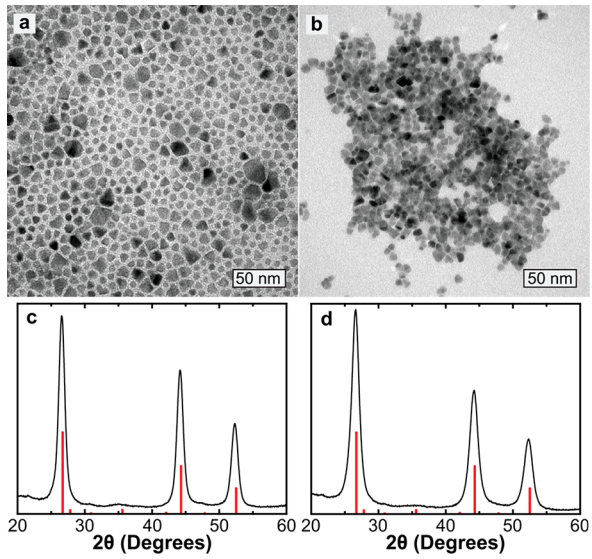

Figure 6. (a) TEM image of as-synthesized $CuInSe_2$ nanocrystals. (b) TEM image of the $CuInSe_2$ nanocrystals after a TOP and 20% wt I_2 ligand exchange. (c) XRD pattern of as-synthesized $CuInSe_2$ nanocrystals. (d) XRD pattern of the $CuInSe_2$ nanocrystals after a TOP and 20% wt I_2 ligand exchange. PDF 01-073-6321 is used as the chalcopyrite $CuInSe_2$ reference XRD pattern, indicated by red drop lines.

structure and morphology (histograms of the size distribution obtained by TEM are available as Supporting Information). The mode of the size distribution (or peak in the frequency distribution) is between 8 and 9 nm before and after the ligand exchange. Before the ligand exchange, the sample contains several larger nanocrystals with diameters of ≤20 nm. After the ligand exchange process, these larger nanocrystals have been removed and the largest nanocrystals are only 13 nm in diameter. This is likely due to the relatively poor dispersibility of the larger nanocrystals and corresponds to the observed mass loss during the exchange process. We also attempted the exchange of OLAm and DPP with an X-type ligand, StAc. Without the addition of I_2, there is no ligand exchange. When I_2 was present, the nanocrystals precipitated, indicating that I_2 displaced OLAm and DPP but StAc did not bond to the nanocrystal surface [see the Supporting Information for the related ^{1}H NMR spectra (Figure S3)].

Figure 7 shows XPS data of the $CuInSe_2$ nanocrystals after I_2 was used to induce exchange of OLAm and DPP ligands with TOP. Even after purification of the nanocrystals by antisolvent precipitation, there is a significant amount of charge neutral iodine remaining on the nanocrystal surface. Previous studies of single-crystal $CuInSe_2$ substrates have shown that I_2 exhibits dissociative adsorption at room temperature with I adatoms bonded preferentially to Cu sites.[60] The binding energy of the I 3d 5/2 peak (619.3 eV) is also consistent with values reported for iodine atoms on noble metal surfaces.[70,71] The Cu 2p, In 3d, and Se 3d XPS peaks all have similar relative intensity and binding energies before and after ligand exchange, indicating that no significant change has occurred to the nanocrystal surface other than the addition of I. Table 1 shows a comparison of the elemental composition of the nanocrystals before and after ligand exchange. Both XPS and

DOI: 10.1021/acs.chemmater.8b04016
Chem. Mater. 2018, 30, 8359–8367

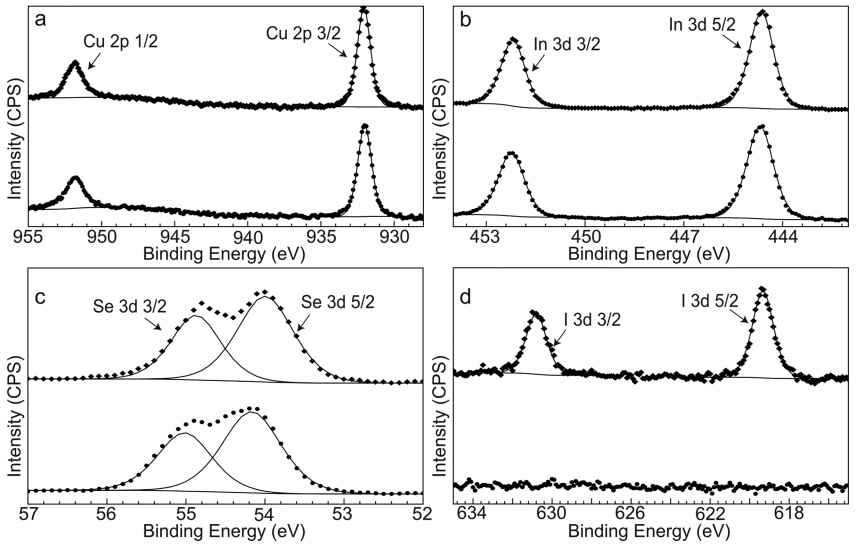

Figure 7. XPS data for $CuInSe_2$ nanocrystals as synthesized (bottom) and after a 20 wt % I_2 and TOP ligand exchange (top). Each region corresponds to the following atomic orbitals: (a) Cu 2p, (b) In 3d, (c) Se 3d, and (d) I 3d.

Table 1. Composition of $CuInSe_2$ Nanocrystals Determined by Integrating the XPS Data in Figure 7 and Composition of $CuInSe_2$ Nanocrystals Determined by ICP-AES[a]

Surface Sensitive $CuInSe_2$ Composition Determined by XPS				
	Cu	In	Se	I
as synthesized	0.69	1.36	2.00	–
exchanged	0.72	1.30	2.00	0.20
Bulk $CuInSe_2$ Composition Determined by ICP-AES				
	Cu	In	Se	
as synthesized	0.80 ± 0.01	1.06 ± 0.02	2.00 ± 0.03	
exchanged	0.81 ± 0.01	1.06 ± 0.01	2.00 ± 0.02	

[a]The XPS measurements are more sensitive to the species at the nanocrystal surface, while ICP-AES measures the total composition in the sample.

ICP-AES indicate that the $CuInSe_2$ nanocrystals are rich in In and deficient in Cu, which is indicative of $In_{Cu}+2V_{Cu}$ defect pairs that have an unusually low formation energy in this class of materials.[72−75] The XPS data indicate that these defect pairs are more prevalent on the surface on the nanocrystals, which is also common in $CuInSe_2$.[76−80] The Cu 2p, In 3d, and Se 3d spectra and the overall nanocrystal composition measured by ICP-AES remain unaffected by the ligand exchange, indicating that the $CuInSe_2$ nanocrystal surface composition is not affected by exposure to I_2 and the nanocrystals are stoichiometric and charge neutral, which is also consistent with dative L-type bonding of OLAm, DPP, TOP, and ODT and bonding of I_2 as a charge neutral Z-type ligand.[48−50]

CONCLUSIONS

OLAm and DPP are tightly bonded L-type ligands on $CuInSe_2$ nanocrystals. The addition of I_2 dislodges both DPP and OLAm from the nanocrystal surface and chemisorbs as a charge neutral Z-type ligand. This is an example of the facile exchange between L-type and Z-type ligands at a nanocrystal surface. The incorporation of I_2 into solution ligand exchange procedures can be used to dislodge the native ligands and facilitate complete ligand exchange. These results support previous findings showing facile exchange between Z-type and L-type ligands and indicate that the presence of the Z-type ligand is necessary to facilitate exchange between tightly bound L-type ligands.

ASSOCIATED CONTENT

Supporting Information

The Supporting Information is available free of charge on the ACS Publications website at DOI: 10.1021/acs.chemmater.8b04016.

^{1}H NMR spectra of the ligands used in the study, full ^{1}H NMR spectra obtained from the heating experiments in Figure 2, ^{1}H NMR spectra showing that OLAm does not exchange with stearic acid, FTIR spectra of $CuInSe_2$ nanocrystals before and after ligand exchange with TOP and I_2, histograms of $CuInSe_2$ nanocrystal sizes measured by TEM before and after complete ligand exchange with TOP and I_2, and XRD data of the red solid byproduct ($CuISe_3$) obtained when $CuInSe_2$ nanocrystals were exposed to very high concentrations of I_2 (PDF)

AUTHOR INFORMATION

Corresponding Author

*E-mail: korgel@che.utexas.edu. Phone: +1-512-471-5633.

ORCID

Brian A. Korgel: 0000-0001-6242-7526

Notes

The authors declare no competing financial interest.

ACKNOWLEDGMENTS

The authors thank Hugo Celio for help with XPS measurements and Steven Sorey for help with measuring the ^{1}H NMR spectra with *in situ* heating. Financial support was provided by the Robert A. Welch Foundation (F-1464) and the National Science Foundation Industry/University Cooperative Research Center on Next Generation Photovoltaics (IIP-1134849, IIP-1540028, IIP-1822206).

DOI: 10.1021/acs.chemmater.8b04016
Chem. Mater. 2018, 30, 8359−8367

REFERENCES

(1) Panthani, M. G.; Akhavan, V.; Goodfellow, B.; Schmidtke, J. P.; Dunn, L.; Dodabalapur, A.; Barbara, P. F.; Korgel, B. A. Synthesis of $CuInS_2$, $CuInSe_2$, and $Cu(In_xGa_{1-x})Se_2$ (CIGS) Nanocrystal "Inks" for Printable Photovoltaics. *J. Am. Chem. Soc.* **2008**, *130*, 16770−16777.

(2) Guo, Q.; Kim, S. J.; Kar, M.; Shafarman, W. N.; Birkmire, R. W.; Stach, E. A.; Agrawal, R.; Hillhouse, H. W. Development of $CuInSe_2$ Nanocrystal and Nanoring Inks for Low-Cost Solar Cells. *Nano Lett.* **2008**, *8*, 2982−2987.

(3) Berends, A. C.; van der Stam, W.; Akkerman, Q. A.; Meeldijk, J. D.; van der Lit, J.; de Mello Donega, C. Anisotropic 2D Cu2-xSe Nanocrystals from Dodecaneselenol and Their Conversion to CdSe and $CuInSe_2$ Nanoparticles. *Chem. Mater.* **2018**, *30*, 3836−3846.

(4) Tappan, B. A.; Barim, G.; Kwok, J. C.; Brutchey, R. L. Utilizing Diselenide Precursors toward Rationally Controlled Synthesis of Metastable $CuInSe_2$ Nanocrystals. *Chem. Mater.* **2018**, *30*, 5704−5713.

(5) Maes, J.; Dierick, R.; Capon, B.; Detavernier, C.; Hens, Z. Se-containing Inks for the Formation of $CuInSe_2$ Films without Gas-Phase Selenization. *Sol. Energy Mater. Sol. Cells* **2016**, *145*, 126−133.

(6) Liu, Y.; Yao, D.; Shen, L.; Zhang, H.; Zhang, X.; Yang, B. Alkylthiol-Enabled Se Powder Dissolution in Oleylamine at Room Temperature for the Phosphine-Free Synthesis of Copper-Based Quaternary Selenide Nanocrystals. *J. Am. Chem. Soc.* **2012**, *134*, 7207−7210.

(7) Ibanez, M.; Zamani, R.; Li, W.; Cadavid, D.; Gorsse, S.; Katcho, N. A.; Shavel, A.; Lopez, A. M.; Morante, J. R.; Arbiol, J.; Cabot, A. Crystallographic Control at the Nanoscale to Enhance Functionality: Polytypic Cu_2GeSe_3 Nanoparticles as Thermoelectric Materials. *Chem. Mater.* **2012**, *24*, 4615−4622.

(8) Lauth, J.; Marbach, J.; Meyer, A.; Dogan, S.; Klinke, C.; Kornowski, A.; Weller, H. Virtually Bare Nanocrystal Surfaces: Significantly Enhanced Electrical Transport in $CuInSe_2$ and $CuIn_{1-x}Ga_xSe_2$ Thin Films upon Ligand Exchange with Thermally Degradable 1-Ethyl-5-Thiotetrazole. *Adv. Funct. Mater.* **2014**, *24*, 1081−1088.

(9) Singh, M.; Jiu, J.; Sugahara, T.; Suganuma, K. Thin-Film Copper Indium Gallium Selenide Solar Cells Based on Low-Temperature All-Printing Process. *ACS Appl. Mater. Interfaces* **2014**, *6*, 16297−16303.

(10) Sandroni, M.; Wegner, K. D.; Aldakov, D.; Reiss, P. Prospects of Chalcopyrite-Type Nanocrystals for Energy Applications. *ACS Energy Lett.* **2017**, *2*, 1076−1088.

(11) Zhong, H.; Wang, Z.; Bovero, E.; Lu, Z.; van Veggel, F. C. J. M.; Scholes, G. D. Colloidal $CuInSe_2$ Nanocrystals in the Quantum Confinement Regime: Synthesis, Optical Properties, and Electroluminescence. *J. Phys. Chem. C* **2011**, *115*, 12396−12402.

(12) Pinchetti, V.; Lorenzon, M.; McDaniel, H.; Lorenzi, R.; Meinardi, F.; Klimov, V. I.; Brovelli, S. Spectro-electrochemical Probing of Intrinsic and Extrinsic Processes in Exciton Recombination in I-III-VI_2 Nanocrystals. *Nano Lett.* **2017**, *17*, 4508−4517.

(13) Allen, P. M.; Bawendi, M. G. Ternary I-III-VI Quantum Dots Luminescent in the Red to Near-Infrared. *J. Am. Chem. Soc.* **2008**, *130*, 9240−9241.

(14) Chen, B.; Pradhan, N.; Zhong, H. From Large-Scale Synthesis to Lighting Device Applications of Ternary I-III-VI Semiconductor Nanocrystals: Inspiring Greener Material Emitters. *J. Phys. Chem. Lett.* **2018**, *9*, 435−445.

(15) Nagamine, G.; Nunciaroni, H. B.; McDaniel, H.; Efros, A. L.; de Brito Cruz, C. H.; Padilha, L. A. Evidence of Band-Edge Hole Levels Inversion in Spherical $CuInS_2$ Quantum Dots. *Nano Lett.* **2018**, *18*, 6353−6359.

(16) McHugh, K. J.; Jing, L.; Behrens, A. M.; Jayawardena, S.; Tang, W.; Gao, M.; Langer, R.; Jaklenec, A. Biocompatible Semiconductor Quantum Dots as Cancer Imaging Agents. *Adv. Mater.* **2018**, *30*, 1706356.

(17) Yarema, O.; Yarema, M.; Wood, V. Tuning the Composition of Multicomponent Semiconductor Nanocrystals: The Case of I-III-VI Materials. *Chem. Mater.* **2018**, *30*, 1446−1461.

(18) Cassette, E.; Pons, T.; Bouet, C.; Helle, M.; Bezdetnaya, L.; Marchal, F.; Dubertret, B. Synthesis and Characterization of Near-Infrared Cu-In-Se/ZnS Core/Shell Quantum Dots for In vivo Imaging. *Chem. Mater.* **2010**, *22*, 6117−6124.

(19) Allen, P. M.; Bawendi, M. G. Ternary I−III−VI Quantum Dots Luminescent in the Red to Near-Infrared. *J. Am. Chem. Soc.* **2008**, *130*, 9240−9241.

(20) Yarema, O.; Bozyigit, D.; Rousseau, I.; Nowack, L.; Yarema, M.; Heiss, W.; Wood, V. Highly Luminescent, Size and Shape Tunable Copper Indium Selenide Based Colloidal Nanocrystals. *Chem. Mater.* **2013**, *25*, 3753−3757.

(21) Akhavan, V. A.; Panthani, M. G.; Goodfellow, B. W.; Reid, D. K.; Korgel, B. A. Thickness-Limited Performance of $CuInSe_2$ Nanocrystal Photovoltaic Devices. *Opt. Express* **2010**, *18*, A411.

(22) Akhavan, V. A.; Goodfellow, B. W.; Panthani, M. G.; Steinhagen, C.; Harvey, T. B.; Stolle, C. J.; Korgel, B. A. Colloidal CIGS and CZTS Nanocrystals: A Precursor Route to Printed Photovoltaics. *J. Solid State Chem.* **2012**, *189*, 2−12.

(23) Meinardi, F.; McDaniel, H.; Carulli, F.; Colombo, A.; Velizhanin, K. A.; Makarov, N. S.; Simonutti, R.; Klimov, V. I.; Brovelli, S. Highly Efficient Large-Area Colourless, Luminescent Solar Concentrators Using Heavy-Metal-Free Colloidal Quantum Dots. *Nat. Nanotechnol.* **2015**, *10*, 878−885.

(24) Boles, M. A.; Ling, D.; Hyeon, T.; Talapin, D. V. The Surface Science of Nanocrystals. *Nat. Mater.* **2016**, *15*, 364−364.

(25) Voggu, V. R.; Sham, J.; Pfeffer, S.; Pate, J.; Fillip, L.; Harvey, T. B.; Brown, R. M.; Korgel, B. A. Flexible $CuInSe_2$ Nanocrystal Solar Cells on Paper. *ACS Energy Lett.* **2017**, *2*, 574−581.

(26) Pernik, D. R.; Gutierrez, M.; Thomas, C.; Voggu, V. R.; Yu, Y.; van Embden, J.; Topping, A. J.; Jasieniak, J. J.; Vanden Bout, D. A.; Lewandowski, R.; et al. Plastic Microgroove Solar Cells Using $CuInSe_2$ Nanocrystals. *ACS Energy Lett.* **2016**, *1*, 1021−1027.

(27) Stolle, C. J.; Panthani, M. G.; Harvey, T. B.; Akhavan, V. A.; Korgel, B. A. Comparison of the Photovoltaic Response of Oleylamine and Inorganic Ligand-Capped $CuInSe_2$ Nanocrystals. *ACS Appl. Mater. Interfaces* **2012**, *4*, 2757−2761.

(28) Harvey, T. B.; Mori, I.; Stolle, C. J.; Bogart, T. D.; Ostrowski, D. P.; Glaz, M. S.; Du, J.; Pernik, D. R.; Akhavan, V. A.; Kesrouani, H.; Vanden Bout, D. A.; Korgel, B. A. Copper Indium Gallium Selenide (CIGS) Photovoltaic Devices Made Using Multistep Selenization of Nanocrystal Films. *ACS Appl. Mater. Interfaces* **2013**, *5*, 9134−9140.

(29) Lan, X.; Voznyy, O.; García de Arquer, F. P.; Liu, M.; Xu, J.; Proppe, A. H.; Walters, G.; Fan, F.; Tan, H.; Liu, M.; et al. 10.6% Certified Colloidal Quantum Dot Solar Cells via Solvent-Polarity-Engineered Halide Passivation. *Nano Lett.* **2016**, *16*, 4630−4634.

(30) Chuang, C.-H. M.; Brown, P. R.; Bulović, V.; Bawendi, M. G. Improved Performance and Stability in Quantum Dot Solar Cells through Band Alignment Engineering. *Nat. Mater.* **2014**, *13*, 796−801.

(31) Tang, J.; Kemp, K. W.; Hoogland, S.; Jeong, K. S.; Liu, H.; Levina, L.; Furukawa, M.; Wang, X.; Debnath, R.; Cha, D.; et al. Colloidal-Quantum-Dot Photovoltaics Using Atomic-Ligand Passivation. *Nat. Mater.* **2011**, *10*, 765−771.

(32) Ning, Z.; Voznyy, O.; Pan, J.; Hoogland, S.; Adinolfi, V.; Xu, J.; Li, M.; Kirmani, A. R.; Sun, J.-P.; Minor, J.; et al. Air-Stable n-Type Colloidal Quantum Dot Solids. *Nat. Mater.* **2014**, *13*, 822−828.

(33) Weidman, M. C.; Yager, K. G.; Tisdale, W. A. Interparticle Spacing and Structural Ordering in Superlattice PbS Nanocrystal Solids Undergoing Ligand Exchange. *Chem. Mater.* **2015**, *27*, 474−482.

(34) Lan, X.; Voznyy, O.; Kiani, A.; Garcia de Arquer, F. P.; Saud Abbas, A.; Kim, G.-H.; Liu, M.; Yang, Z.; Walters, G.; Xu, J.; Yuan, M.; Ning, Z.; Fan, F.; Kanjanaboos, P.; Kramer, I.; Zhitomirsky, D.; Lee, P.; Perelgut, A.; Hoogland, S.; Sargent, E. H. Passivation Using Molecular Halides Increases Quantum Dot Solar Cell Performance. *Adv. Mater.* **2016**, *28*, 299−304.

DOI: 10.1021/acs.chemmater.8b04016
Chem. Mater. 2018, 30, 8359−8367

(35) Draguta, S.; McDaniel, H.; Klimov, V. I. Tuning Carrier Mobilities and Polarity of Charge Transport in Films of $CuInSe_xS_{2-x}$ Quantum Dots. *Adv. Mater.* **2015**, *27*, 1701−1705.
(36) Reifsnyder, D. C.; Ye, X.; Gordon, T. R.; Song, C.; Murray, C. B. Three-Dimensional Self-Assembly of Chalcopyrite Copper Indium Diselenide Nanocrystals into Oriented Films. *ACS Nano* **2013**, *7*, 4307−4315.
(37) Owen, J. S.; Park, J.; Trudeau, P.-E.; Alivisatos, A. P. Reaction Chemistry and Ligand Exchange at Cadmium−Selenide Nanocrystal Surfaces. *J. Am. Chem. Soc.* **2008**, *130*, 12279−12281.
(38) Gomes, R.; Hassinen, A.; Szczygiel, A.; Zhao, Q.; Vantomme, A.; Martins, J. C.; Hens, Z. Binding of Phosphonic Acids to CdSe Quantum Dots: A Solution NMR Study. *J. Phys. Chem. Lett.* **2011**, *2*, 145−152.
(39) Anderson, N. C.; Owen, J. S. Soluble, Chloride-Terminated CdSe Nanocrystals: Ligand Exchange Monitored by ^{1}H and ^{31}P NMR Spectroscopy. *Chem. Mater.* **2013**, *25*, 69−76.
(40) Fritzinger, B.; Capek, R. K.; Lambert, K.; Martins, J. C.; Hens, Z. Utilizing Self-Exchange To Address the Binding of Carboxylic Acid Ligands to CdSe Quantum Dots. *J. Am. Chem. Soc.* **2010**, *132*, 10195−10201.
(41) Turo, M. J.; Shen, X.; Brandon, N. K.; Castillo, S.; Fall, A. M.; Pantelides, S. T.; Macdonald, J. E. Dual-Mode Crystal-Bound and X-Type Passivation of Quantum Dots. *Chem. Commun.* **2016**, *52*, 12214−12217.
(42) Moreels, I.; Fritzinger, B.; Martins, J. C.; Hens, Z. Surface Chemistry of Colloidal PbSe Nanocrystals. *J. Am. Chem. Soc.* **2008**, *130*, 15081−15086.
(43) De Roo, J.; Justo, Y.; De Keukeleere, K.; Van den Broeck, F.; Martins, J. C.; Van Driessche, I.; Hens, Z. Carboxylic-Acid-Passivated Metal Oxide Nanocrystal: Ligand Exchange Characteristics of a New Binding Motif. *Angew. Chem., Int. Ed.* **2015**, *54*, 6488−6491.
(44) De Roo, J.; Van den Broeck, F.; De Keukeleere, K.; Martins, J. C.; Van Driessche, I.; Hens, Z. Unravelling the Surface Chemistry of Metal Oxide Nnaocrystals, the Role of Acids and Bases. *J. Am. Chem. Soc.* **2014**, *136*, 9650−9657.
(45) De Roo, J.; Ibanez, M.; Geiregat, P.; Nedelcu, G.; Walravens, W.; Maes, J.; Martins, J. C.; Van Driessche, I.; Kovalenko, M. V.; Hens, Z. Highly Dynamic Ligand Binding and Light Absorption Coefficient of Cesium Lead Bromide Perovskite Nanocrystals. *ACS Nano* **2016**, *10*, 2071−2081.
(46) Turo, M. J.; Macdonald, J. E. Crystal-Bound *vs* Surface-Bound Thiols on Nanocrystals. *ACS Nano* **2014**, *8*, 10205−10213.
(47) Dierick, R.; Van den Broeck, F.; De Nolf, K.; Zhao, Q.; Vantomme, A.; Martins, J. C.; Hens, Z. Surface Chemistry of $CuInS_2$ Colloidal Nanocrystals, Tight Binding of L-Type Ligands. *Chem. Mater.* **2014**, *26*, 5950−5957.
(48) Green, M. L. H. A. New Approach to the Formal Classification of Covalent Compounds of the Elements. *J. Organomet. Chem.* **1995**, *500* (1−2), 127−148.
(49) Zhou, Y.; Wang, F.; Buhro, W. E. Large Exciton Energy Shifts by Reversible Surface Exchange in 2D II-VI Nanocrystals. *J. Am. Chem. Soc.* **2015**, *137*, 15198−15208.
(50) Owen, J. The Coordination Chemistry of Nanocrystal Surfaces. *Science* **2015**, *347*, 615−616.
(51) Yao, Y.; Zhou, Y.; Sanderson, W. M.; Loomis, R. A.; Buhro, W. E. Metal-Halide-Ligated Cadmium Selenide Quantum Belts by Facile Surface Exchange. *Chem. Mater.* **2018**, *30*, 2848−2857.
(52) Drijvers, E.; De Roo, J.; Martins, J. C.; Infante, I.; Hens, Z. Ligand Displacement Exposes Binding Site Heterogeneity on CdSe Nanocrystal Surfaces. *Chem. Mater.* **2018**, *30*, 1178−1186.
(53) Donakowski, M. D.; Godbe, J. M.; Sknepnek, R.; Knowles, K. E.; Olvera de la Cruz, M.; Weiss, E. A. A Quantitative Description of the Binding Equilibria of para-Substituted Aniline Ligands and CdSe Quantum Dots. *J. Phys. Chem. C* **2010**, *114*, 22526−22534.
(54) Anderson, N. C.; Owen, J. S. Soluble, Chloride-Terminated CdSe Nanocrystals: Ligand Exchange Monitored by ^{1}H and ^{31}P NMR Spectroscopy. *Chem. Mater.* **2013**, *25*, 69−76.
(55) Moreels, I.; Martins, J. C.; Hens, Z. Ligand Adsorption/Desorption on Sterically Stabilized InP Colloidal Nanocrystals: Observation and Thermodynamic Analysis. *ChemPhysChem* **2006**, *7*, 1028−1031.
(56) Morris-Cohen, A. J.; Malicki, M.; Peterson, M. D.; Slavin, J. W. J.; Weiss, E. A. Chemical, Structural, and Quantitative Analysis of the Ligand Shells of Colloidal Quantum Dots. *Chem. Mater.* **2013**, *25*, 1155−1165.
(57) Dilena, E.; Xie, Y.; Brescia, R.; Prato, M.; Maserati, L.; Krahne, R.; Paolella, A.; Bertoni, G.; Povia, M.; Moreels, I.; Manna, L. $CuIn_xGa_{1-x}S_2$ Nanocrystals with Tunable Composition and Band Gap Synthesized via a Phosphine-Free and Scalable Procedure. *Chem. Mater.* **2013**, *25*, 3180−3187.
(58) Tavasoli, E.; Guo, Y.; Kunal, P.; Grajeda, J.; Gerber, A.; Vela, J. Surface Doping Quantum Dots with Chemically Active Native Ligands: Controlling Valence without Ligand Exchange. *Chem. Mater.* **2012**, *24*, 4231−4241.
(59) Hens, Z.; Martins, J. C. A Solution NMR Toolbox for Characterizing the Surface Chemistry of Colloidal Nanocrystals. *Chem. Mater.* **2013**, *25*, 1211−1221.
(60) Sander, M.; Jaegermann, W.; Lewerenz, H. J. Site-Specific Surface Interaction of Adsorbed Water and Halogens on Copper Indium Selenide ($CuInSe_2$) Surfaces. *J. Phys. Chem.* **1992**, *96*, 782−790.
(61) Panthani, M. G.; Stolle, C. J.; Reid, D. K.; Rhee, D. J.; Harvey, T. B.; Akhavan, V. A.; Yu, Y.; Korgel, B. A. $CuInSe_2$ Quantum Dot Solar Cells with High Open-Circuit Voltage. *J. Phys. Chem. Lett.* **2013**, *4*, 2030−2034.
(62) The total weight of the $CuInSe_2$ nanocrystals is composed of 10% by mass of OLAm. The amount of OLAm in 50 mg of $CuInSe_2$ nanocrystals dispersed in chloroform-*d* was determined from the NMR spectra by comparing the intensity of the ^{1}H NMR signal of OLAm vinylic protons at δ 5.36 ppm to the intensity of the TMS peak at δ 0 ppm.
(63) Castle, J. E.; Chapman-Kpodo, H.; Proctor, A.; Salvi, A. Curve-Fitting in XPS Using Extrinsic and Intrinsic Background Structure. *J. Electron Spectrosc. Relat. Phenom.* **2000**, *106*, 65−80.
(64) Shirley, D. A. High-Resolution X-Ray Photoemission Spectrum of the Valence Bands of Gold. *Phys. Rev. B* **1972**, *5*, 4709−4714.
(65) Kohiki, S.; Nishitani, M.; Negami, T.; Wada, T. X-Ray Photoelectron Spectroscopy of $CuInSe_2$. *Phys. Rev. B: Condens. Matter Mater. Phys.* **1992**, *45*, 9163−9168.
(66) Badia, A.; Gao, W.; Singh, S.; Demers, L.; Cuccia, L.; Reven, L. Structure and chain dynamics of alkanethiol-capped gold colloids. *Langmuir* **1996**, *12*, 1262−1269.
(67) Korgel, B. A.; Fullam, S.; Connolly, S.; Fitzmaurice, D. Assembly and Self-Organization of Silver Nanocrystal Superlattices: Ordered "Soft Spheres. *J. Phys. Chem. B* **1998**, *102*, 8379−8388.
(68) Terrill, R. H.; Postlethwaite, T. A.; Chen, C.-H.; Poon, C.-D.; Terzis, A.; Chen, A.; Hutchison, J. E.; Clark, M. R.; Wignall, G. Monolayers in Three Dimensions: NMR, SAXS, Thermal, and Electron Hopping Studies of Alkanethiol Stabilized Gold Clusters. *J. Am. Chem. Soc.* **1995**, *117*, 12537−12548.
(69) Marbella, L. E.; Millstone, J. E. NMR Techniques for Noble Metal Nanoparticles. *Chem. Mater.* **2015**, *27*, 2721−2739.
(70) Berry, G. M.; Bravo, B. G.; Bothwell, M. E.; Cali, G. J.; Harris, J. E.; Mebrahtu, T.; Michelhaugh, S. L.; Rodriguez, J. F.; Soriaga, M. P. Spectroscopic and Electrochemical Studies of Iodine Coordinated to Noble-Metal Electrode Surfaces. *Langmuir* **1989**, *5*, 707−713.
(71) Wertheim, G. K.; DiCenzo, S. B.; Buchanan, D. N. E. Core-Electron Spectroscopy of Adsorbate Ions: Iodine on Ag(111). *Phys. Rev. B: Condens. Matter Mater. Phys.* **1982**, *25*, 3020−3025.
(72) Zhang, S. B.; Wei, S.-H.; Zunger, A.; Katayama-Yoshida, H. Defect Physics of the $CuInSe_2$ Chalcopyrite Semiconductor. *Phys. Rev. B: Condens. Matter Mater. Phys.* **1998**, *57*, 9642−9656.
(73) Zhang, S. B.; Wei, S.-H.; Zunger, A. Stabilization of Ternary Compounds via Ordered Arrays of Defect Pairs. *Phys. Rev. Lett.* **1997**, *78*, 4059−4062.

DOI: 10.1021/acs.chemmater.8b04016
Chem. Mater. 2018, 30, 8359−8367

(74) Allen, P. M.; Bawendi, M. G. Ternary I−III−VI Quantum Dots Luminescent in the Red to Near-Infrared. *J. Am. Chem. Soc.* **2008**, *130*, 9240−9241.
(75) Yarema, O.; Yarema, M.; Wood, V. Tuning the Composition of Multicomponent Semiconductor Nanocrystals: The Case of I−III−VI Materials. *Chem. Mater.* **2018**, *30*, 1446−1461.
(76) Yan, Y.; Jiang, C.-S.; Noufi, R.; Wei, S.-H.; Moutinho, H. R.; Al-Jassim, M. M. Electrically Benign Behavior of Grain Boundaries in Polycrystalline $CuInSe_2$ Films. *Phys. Rev. Lett.* **2007**, *99*, 235504.
(77) Kohiki, S.; Nishitani, M.; Negami, T.; Wada, T. X-Ray Photoelectron Spectroscopy of $CuInSe_2$. *Phys. Rev. B: Condens. Matter Mater. Phys.* **1992**, *45*, 9163−9168.
(78) Sobol, P. E.; Nelson, A. J.; Schwerdtfeger, C. R.; Stickle, W. F.; Moulder, J. F. Single Crystal $CuInSe_2$ Analysis by High Resolution XPS. *Surf. Sci. Spectra* **1992**, *1*, 393−397.
(79) Akhavan, V. A.; Harvey, T. B.; Stolle, C. J.; Ostrowski, D. P.; Glaz, M. S.; Goodfellow, B. W.; Panthani, M. G.; Reid, D. K.; VandenBout, D. A.; Korgel, B. A. Influence of Composition on the Performance of Sintered $Cu(In,Ga)Se_2$ Nanocrystal Thin-Film Photovoltaic Devices. *ChemSusChem* **2013**, *6*, 481−486.
(80) Kötschau, I. M.; Schock, H. W. Depth Profile of the Lattice Constant of the Cu-Poor Surface Layer in $(Cu_2Se)_{1-x}(In_2Se_3)_x$ Evidenced by Grazing Incidence X-Ray Diffraction. *J. Phys. Chem. Solids* **2003**, *64*, 1559−1563.

DOI: 10.1021/acs.chemmater.8b04016
Chem. Mater. 2018, 30, 8359−8367